crystals

MDPI

Article

Computational Study of Molecular Interactions in $ZnCl_2(urea)_2$ Crystals as Precursors for Deep Eutectic Solvents

Adrian Malinowski and Maciej Śmiechowski *

Department of Physical Chemistry, Faculty of Chemistry, Gdańsk University of Technology, Narutowicza 11/12, 80-233 Gdańsk, Poland

* Correspondence: maciej.smiechowski@pg.edu.pl

Abstract: Deep eutectic solvents (DESs) are now enjoying an increased scientific interest due to their interesting properties and growing range of possible applications. Computational methods are at the forefront of deciphering their structure and dynamics. Type IV DESs, composed of metal chloride and a hydrogen bond donor, are among the less studied systems when it comes to their understanding at a molecular level. An important example of such systems is the zinc chloride–urea DES, already used in chemical synthesis, among others. In this paper, the $ZnCl_2(urea)_2$ crystal is studied from the point of view of its structure, infrared spectrum, and intermolecular interactions using periodic density functional theory and non-covalent interactions analysis. The two main structural motifs found in the crystal are a strongly hydrogen-bonded urea dimer assisted by chloride anions and a tetrahedral Zn(II) coordination complex. The crystal is composed of two interlocking parallel planes connected via the zinc cations. The infrared spectrum and bond lengths suggest a partially covalent character of the Zn–Cl bonds. The present analysis has far-reaching implications for the liquid $ZnCl_2$–urea DES, explaining its fluidity, expected microstructure, and low conductivity, among others.

Keywords: zinc chloride; urea; deep eutectic solvents; density functional theory; non-covalent interactions

check for updates

Citation: Malinowski, A.; Śmiechowski, M. Computational Study of Molecular Interactions in $ZnCl_2(urea)_2$ Crystals as Precursors for Deep Eutectic Solvents. *Crystals* **2024**, *14*, 641. https://doi.org/10.3390/cryst14070641

Academic Editor: Antonio Frontera

Received: 22 June 2024
Revised: 5 July 2024
Accepted: 9 July 2024
Published: 11 July 2024

Copyright: © 2024 by the authors. Licensee MDPI, Basel, Switzerland. This article is an open access article distributed under the terms and conditions of the Creative Commons Attribution (CC BY) license (https://creativecommons.org/licenses/by/4.0/).

1. Introduction

Deep eutectic solvents (DESs) are a class of mixtures of two or more components, classified as hydrogen bond donors (HBDs) and acceptors (HBAs), characterized by a significant freezing point depression [1]. Usually, their individual components are solid at room temperature, while mixtures at specific molar ratios around the eutectic point are liquid at such conditions. For example, the first mixture classified as DES, described in 2003 by Abbott et al. [2], which is choline chloride and urea at a 1:2 ratio, exhibits a low melting point long thought to be 285 K, while choline chloride and urea melting points are 575 K and 406 K, respectively. However, these data are now contested, as novel measurement techniques are being introduced. The phase diagram determination of DESs is sensitive to numerous intervening factors, notably water content, tendency to glass formation, and possible thermal decomposition of DES constituents at elevated temperatures. For example, the melting point of choline chloride–urea DES measured using strictly anhydrous compounds in controlled moisture conditions is 305 K [3], while ultrafast scanning calorimetry recently allowed to overcome the decomposition of choline chloride and resulted in an absolute melting point of 687 K [4]. From the point of view of physicochemical properties, DESs are typically viscous, electrically conductive liquids, often exhibiting substantial hygroscopicity [5,6].

Deep eutectic solvents are divided into five general types based on their components [7]. *Type I* consists of quaternary ammonium salt (QAS) and metal chloride (typically the metal is Zn, Sn, Fe, Al, Ga, or In); *type II* contains QAS and hydrated metal chloride (Cr, Co, Cu, Ni, or Fe); *type III* is composed of QAS and HBD, with a wide variety of

organic molecules used in this role; *type IV* consists of a metal halide (Zn or Al) and HBD, and, finally, *type V* [8] is based on non-ionic hydrogen bond donors and acceptors.

Deep eutectic solvents have already found diverse practical uses, as summarized in numerous review articles focusing on different fields of DES applications, including catalytic media for organic syntheses [9,10], liquid–liquid extraction media [11–13], nanotechnology [14], and electrochemistry and power systems [15]. In more general reviews [1,7,16,17], gas separation and desulfurization, biomass processing, and various pharmaceutical and medical research applications are also often mentioned. In the context of metal salt-based DESs, the review by Khalid et al. [18] provides an in-depth summary of the known physicochemical properties and hitherto proposed applications of such systems. Naturally, it is not an exhaustive list of all available reviews on the subject and potential DESs applications.

One of the earlier *type IV* deep eutectic solvents is the $ZnCl_2$–urea in a 1:3.5 ratio, first described in 2007 [19]. When prepared by stirring at an elevated temperature, a transparent liquid forms with a melting point of 282 K. Current research on this and similar systems focuses mostly on their applications rather than theoretical investigations. For example, $ZnCl_2$–urea mixtures were successfully used for lignin processing and modification [20–22], as a solvent for various syntheses [23–26], processing of rubber [27] and poly(ethylene terephthalate) waste [28], nanoparticle synthesis [29], and electrochemical applications [30,31]. As mentioned above, there is a profound lack of theoretical investigations into the nature of *type IV* DESs. An emphasis is put more on the *type III* and *type V* deep eutectics [32,33]. Still, some of the basic physicochemical properties of $ZnCl_2$–urea mixtures were determined, e.g., density, viscosity, conductivity, surface tension, refractive index, and pH [19,26]. However, even in this limited data set, some discrepancies may be observed, such as the reported density at 298 K varying from 1.63 $g{\cdot}cm^{-3}$ [19] to (extrapolated) 1.69 $g{\cdot}cm^{-3}$ [26]. Undoubtedly, DESs based on $ZnCl_2$ are very hygroscopic due to the Zn^{2+} cation's presence and their physical properties are very sensitive to even small amounts of water. Infrared (IR) spectra of DES constituents published previously evidently show H_2O vibrational bands in crystalline $ZnCl_2$ [26] and working in moisture-free conditions is demonstrably necessary to ensure that the properties of DESs, rather than a DES–H_2O system, are measured [3].

Unique properties and highly non-ideal behavior of deep eutectic solvents are most likely caused by a plethora of intermolecular interactions. To probe those, computational chemistry methods are often utilized [32]. While classical molecular dynamics (MD) methods can be applied to investigate the nanostructure of the DES and its properties that rely on ensemble averaging, the investigation of the interactions inside a single 'formula unit' of the DES requires a quantum chemical approach. Usually, density functional theory (DFT) methods (including ab initio molecular dynamics, AIMD) are applied, due to their accuracy and relatively low computational cost. One of the first such investigations of DES properties was the 2016 communication by Zahn et al. [34]. Therein, the authors used ab initio molecular dynamics with periodic boundary conditions (PBCs) for investigating charge transfer in choline chloride/urea system with the rationale that the PBC on even very small systems allows to gain insight on charge spreading inside larger systems. Another example of the application of AIMD methodology in DES studies is the 2020 investigation by Alizadeh et al. [35] of the so-called 'magic compositions' of DESs. Those are specific molar ratios, at which potential DES components are mixed by trial and error, often without exploration of the full solid–liquid phase equilibrum of the system in search of a proper eutectic composition [36]. The choline chloride/ethylene glycol system (which, as it was later discovered [37], is not at a true eutectic composition, showing a problem with its determination) was investigated at various compositions with and without water addition. It was found that a rich network of various hydrogen bonds exists in the DES, but there is nothing peculiar happening at the 'magic' composition. While, as mentioned above, there is a severe lack of theoretical research into the nature of metal-based deep eutectics, there are few results available in the literature. DFT calculations were performed on isolated $ZnCl_2$/choline chloride [38] and $ZnCl_2$/thiazolidine [39] clusters. In the case

of Dhirendra et al., interactions between the DES components were investigated by the Quantum Theory of Atoms in Molecules (QTAIM) and non-covalent interactions analysis, which led to the identification of hydrogen bonding and ionic interaction networks within the studied systems, while Singh et al. applied HOMO–LUMO analysis for the investigation of eutectic formation. This shows that various QM methods can be employed in studies of various deep eutectic solvents, including metal-based ones.

Apart from room-temperature liquids in a narrow range of compositions, the $ZnCl_2$–urea system also exhibits stable crystalline phases, notably $ZnCl_2(urea)_2$ (i.e., 1:2 molar ratio) [40]. Similar crystals are obtainable for other zinc halides, e.g., ZnI_2 [41]. The prepared crystals were free from water, thus offering a unique possibility of studying pristine proto-DES systems. In $ZnCl_2(urea)_2$, each Zn(II) site is roughly tetrahedrally coordinated by two oxygen atoms of urea molecules and two more covalently bound chlorides. Hydrogen bonds between urea and chloride are also observed [40]. According to the only phase diagram published for this system, the composition 1:2 melts at ca. 318 K [19]. This system also forms cocrystals with HCl, $ZnCl_2 \cdot 2\,CO(NH_2)_2 \cdot HCl$, providing an interesting combination of Lewis and Brønsted acidity [42].

Usually, DES clusters for computational investigations are constructed artificially by arbitrarily placing their components, followed by geometry optimization at various levels of theory [38,39]. While proven useful, this does not guarantee, that investigated structures are present in real-life DESs. Utilizing an experimentally determined DES-like $ZnCl_2$–urea crystal structure offers the possibility of theoretical investigation of its geometry as close to the experimental one as possible. The study of this system by means of the periodic DFT method in order to describe the electronic properties of the system, non-covalent interactions, charge distribution, etc., could offer valuable information about the similar, room-temperature DES $ZnCl_2(urea)_{3.5}$, as there are no unique 'magic compositions' for deep eutectic solvents.

2. Computational Methods

The starting point for density functional theory (DFT) calculations is the structure of the $ZnCl_2(urea)_2$ crystal, as determined by the X-ray structure analysis by Furmanova et al. [40]. $ZnCl_2(urea)_2$ crystallizes in the triclinic system with $P\bar{1}$ space group; see Table 1 for lattice constants and further details. There are two $ZnCl_2(urea)_2$ formula units per unit cell. The structure was obtained from the Cambridge Structural Database (deposition no. CSD-1318289) [43].

Table 1. Selected structural parameters of the $ZnCl_2 \cdot 2\,CO(NH_2)_2$ crystal unit cell.

Parameter	Experiment [40]	PBE (This Work)
a/Å	6.275	6.161
b/Å	6.835	6.756
c/Å	11.862	11.913
α/°	79.19	79.91
β/°	72.31	72.04
γ/°	67.21	67.19
V/Å^3	445.444	433.903
d/kg·m^{-3}	1911.6	1962.5
r(Zn···Cl(1))/Å	2.218	2.231
r(Zn···Cl(2))/Å	2.238	2.250
r(Zn···O(1))/Å	1.947	1.964
r(Zn···O(2))/Å	1.986	2.012

All calculations were performed with the CASTEP (v. 23.1) [44] software using the Perdew–Burke–Ernzerhof (PBE) [45] functional with Grimme's D3 dispersion correction using Becke–Johnson damping (DFT-D3BJ) [46,47]. The calculation protocol was as follows: first, the structure of the unit cell was optimized, keeping the $P\bar{1}$ space group fixed. Then,

a 3 × 3 × 2 supercell was constructed from the optimized unit cell. Phonon calculations and lattice energy calculations were performed on this supercell. Additionally, calculations on isolated components for lattice energy estimation were performed. As CASTEP, by definition, always includes periodic boundary conditions, single urea and $ZnCl_2$ were extracted from the above-mentioned supercell and the energy of such isolated molecules was calculated (for components locked in a crystal lattice) and optimized geometries were calculated (for gas phase components). Norm-conserving pseudopotentials generated on the fly [48] were used. While ultrasoft pseudopotentials require a lower plane-wave cut-off value and offer better performance, the current version of CASTEP does not support phonon calculations with ultrasoft pseudopotentials. In all cases, the plane-wave basis set cut-off energy was set to 1200 eV, as this value offered good convergence while still being computationally tractable. As phonon calculations require a high quality of structure optimization, geometry convergence criteria were set as follows: total energy tolerance, 2×10^{-5} eV/atom; maximum force tolerance, 10^{-2} eV/Å; maximal displacement, 10^{-3} Å; and maximal stress component, 0.1 GPa. In order to assure the force convergence to a high accuracy, the maximum force tolerance in the electronic minimization step was set to 5×10^{-4} eV/Å. As a unit cell of the system is elongated in one direction, the Brillouin zone was sampled on a 3 × 3 × 2 Monkhorst–Pack grid [49] in case of calculations on the unit cell. The supercell (built from the optimized unit cell) and individual components were sampled at the Γ-point only. Cif2cell software (v. 2.0.0) [50] was used for supercell building and unit cell manipulation.

QTAIM analysis of critical points of electron density (based on the promolecular approach) [51], as well as non-covalent interaction (NCI) analysis [52] were performed using critic2 (v. 1.1) [53,54]. NCI analysis was performed utilizing promolecular density on the entire supercell. A 400 × 400 × 400 grid was used. The analysis of output files was facilitated by the use of c2x (v. 2.41b) [55]. VMD software (v. 1.9.4) [56] was used for visualizations.

3. Results and Discussion

The lattice constants and other basic parameters of the optimized unit cell are shown in Table 1. Overall, the optimization led to only minor changes in the cell's geometry, proving that the chosen computational protocol is adequate for the present purpose. Using the PBE functional leads to a slight decrease of the cell volume (by about 2.5%) with a corresponding increase of density. Interestingly, although the system density is larger, the tetrahedral coordination shell of Zn(II) is slightly farther away from the cation (by 0.012–0.026 Å), as evidenced by the increased *r*(Zn···Cl) and *r*(Zn···O) distances.

The long-range crystal structure features two, nearly perpendicular planes arranged roughly along *b* and *c* cell vectors, as shown in Figure 1. In both planes, chloride anions are coordinated bidentately by urea molecules through weak hydrogen bonds (HBs) with amine hydrogens. The principal *c*-aligned structural motif (shown in Figure 2a) additionally contains urea dimers bonded through stronger, linear HBs.

Similarly, bidentate chloride complex, albeit lacking urea dimers, is present in the *b*-aligned plane. All urea–chloride interactions are asymmetric, with HBs bent out of linearity by about 30°. The *b*-aligned complex is slightly more asymmetric: the shorter Cl···H bond is 2.36 Å (as compared to 2.38 Å in the *c*-aligned complex), the longer one is 2.64 Å long (2.51 Å in the other complex). Furthermore, the N–H···Cl angles are slightly more asymmetric in this structure, with 155.96° and 142.16° angles, compared to 156.00° and 149.30° in the *c*-aligned complex, respectively, (see Figure 2a).

The perpendicular planes are interconnected through zinc cations coordinated by urea oxygen atoms (see Figure 2b). It should be noted that, in this figure, the Zn(II) atoms are actually out of plane of the main $(Cl^- \cdot CO(NH_2)_2)_2$ structural motif. The interplanar linking is also provided by direct N–H···O urea–urea interactions, which are more distant and strongly bent out of linear arrangement (2.32 Å, 130.02°) when compared to the HBs in the urea dimer. The hydrogen atoms engaged in these interactions are visible in Figure 2a

as the ones not connected with any dotted line. Similar to zinc cations, the accepting urea oxygen atoms (not shown in Figure 2a) are located out of plane.

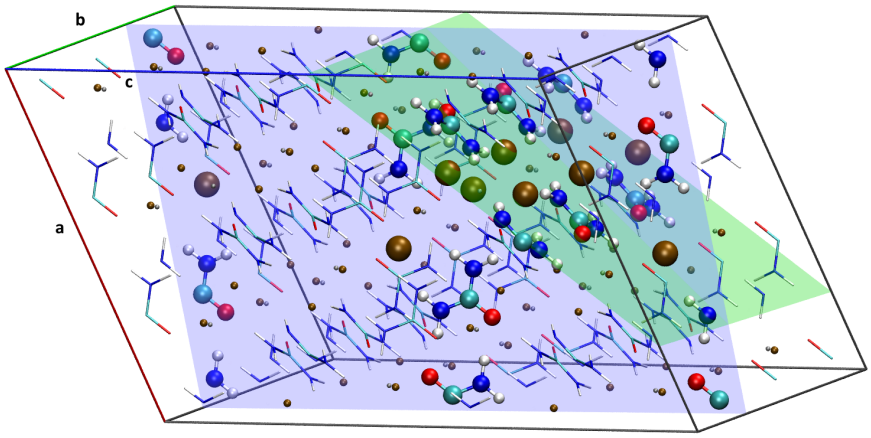


Figure 1. A $3 \times 3 \times 2$ supercell of the $ZnCl_2 \cdot 2\,CO(NH_2)_2$ crystal with two distinct planes shown. The plane of *b*-aligned complexes is shown in green; the *c*-aligned complexes are located along the blue plane. Axes are denoted by letters, as in Table 1. Molecules (atoms) in the highlighted planes are shown in ball-and-stick representation and other molecules (atoms) only as sticks (small balls). Elements are color-coded with the standard VMD coloring as follows: H—white, C—cyan, N—blue, O—red, Cl—tan, and Zn—silver.

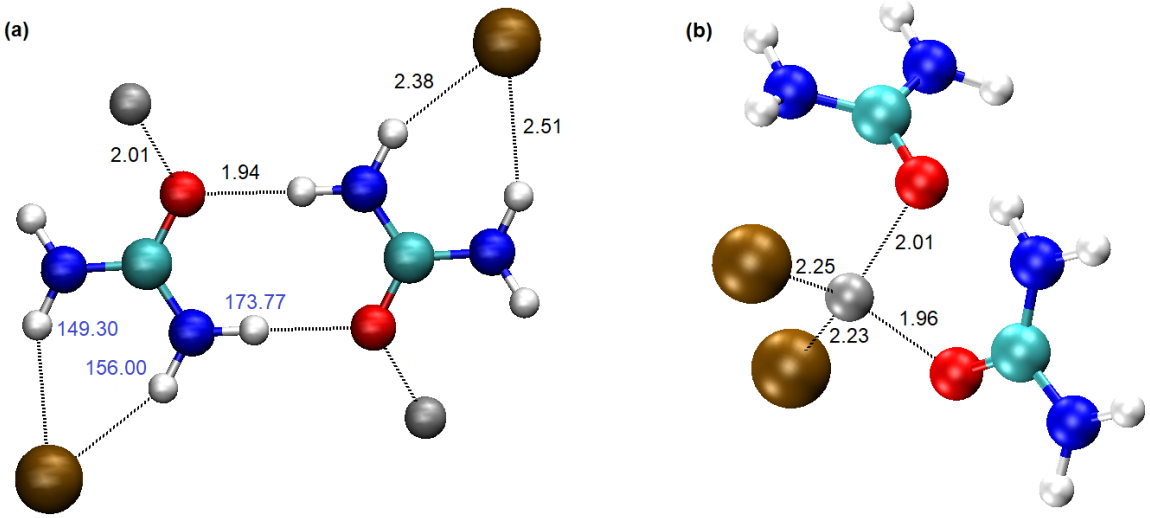


Figure 2. Principal short-range structural motifs present in the $ZnCl_2 \cdot 2\,CO(NH_2)_2$ crystal with intermolecular interactions marked with dotted lines: (**a**) the *c*-aligned urea dimer complex; (**b**) the perpendicular plane linkage through zinc cation. Distances (in Å) are marked in black, and angles (in degrees) marked in blue. Values repeating due to symmetry are not shown for clarity. See Figure 1 for atom color-coding.

The aforementioned hydrogen bonding pattern is confirmed by non-covalent interaction (NCI) analysis (see Figure 3a). In all cases, negative reduced-density gradient zones are present in regions of suspected hydrogen bonding presence. Urea molecules present in parallel planes are held together by van der Waals (vdW) interactions, as shown by large regions of small reduced-density gradients (see Figure 3b). The role of vdW interactions as the main force holding the $ZnCl_2 \cdot 2\,CO(NH_2)_2$ crystal together explains its relatively low melting point (318 K, see above). NCI analysis also reveals that zinc cations are tetrahedrally coordinated and all ligands are strongly interacting with Zn(II), cf. Figure 3b. Observations from NCI analysis are supported by QTAIM analysis—locations of bond

critical points (BCPs) correlate strongly with reduced-density gradient regions highlighted by NCI. Furthermore, information obtained from QTAIM can be used for the estimation of hydrogen bond energy. By examining of various descriptors, Emamian et al. [57] proposed to calculate the interaction energy from electron density at BCPs as the most adequate parameter. Empirical relations were provided separately for neutral and charged hydrogen bonds. In the studied crystal, the O···H interaction is considered neutral, while interactions of hydrogen atoms with the chloride ion are treated as charged. Results for interactions in the $(Cl^- \cdot CO(NH_2)_2)_2$ subunit are shown in Table 2—all of the investigated interactions can be classified as medium-strength hydrogen bonds.

Table 2. Hydrogen bond energies based on electron density at bond critical point.

Interaction	H···X Distance/Å	Electron Density/Å^{-3}	Energy/ kJ·mol^{-1}
O···H	1.94	3.45×10^{-2}	−27.0
Cl···H(1)	2.38	2.23×10^{-2}	−35.5
Cl···H(2)	2.51	1.76×10^{-2}	−29.0

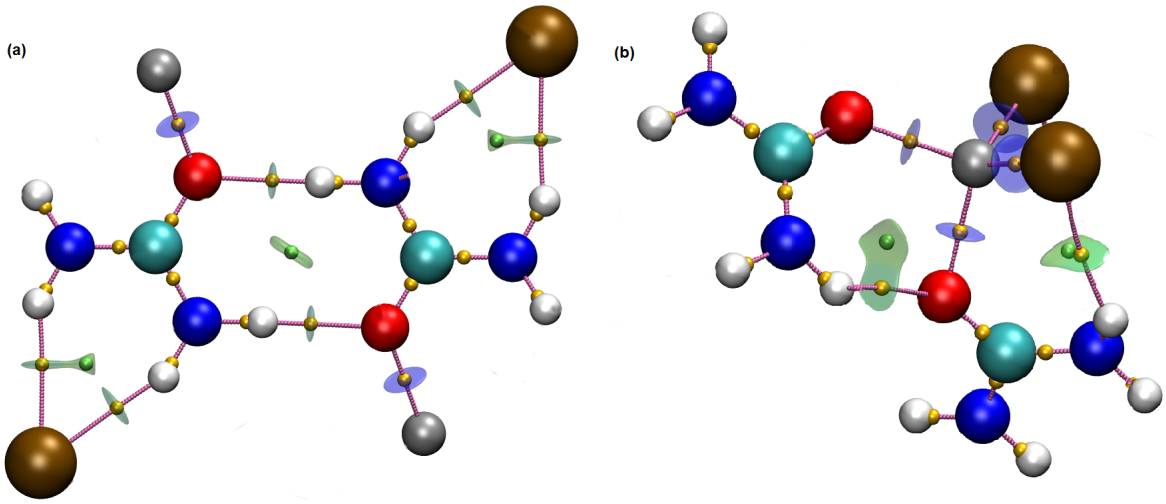


Figure 3. Visualization of non-covalent interactions and QTAIM analysis of main structural motifs in the $ZnCl_2 \cdot 2\,CO(NH_2)_2$ crystal: (**a**) the *c*-aligned urea dimer complex; (**b**) the perpendicular planes linkage through zinc cation. Regions of strong non-covalent interactions and weaker van der Waals interactions are indicated in blue and green, respectively. Bond critical points and ring critical points are marked with yellow and lime spheres, respectively. Bond paths are shown as pink lines. See Figure 1 for atom color-coding.

It is interesting to compare the obtained crystal structure with pure urea crystals (Cambridge Structural Database deposition no. CSD-131762) [58]. Urea crystallizes in the tetragonal crystal system in the $P\bar{4}2_1m$ space group. Urea molecules are located on two perpendicular planes, with ureas within one plane connected by a network of symmetrical bidentate hydrogen bonds 2.07 Å long between amine groups' hydrogens and the oxygen of next molecule. Perpendicular planes are connected with slightly shorter (2.01 Å) HBs. This arrangement looks quite similar to the $ZnCl_2 \cdot 2\,CO(NH_2)_2$ proto-DES structure. Zinc chloride seems to disrupt the pure urea structure with chloride ions inserted between urea molecules. Those replace the role of carbonyl oxygens of urea as linkers, but the hydrogen bonds that they participate in are considerably weaker. Similarly, hydrogen bonds interconnecting perpendicular planes of urea are replaced by coordination interactions through zinc cations.

The length of the Zn···Cl coordination bonds in the studied crystal exhibits very slight asymmetry with two values of 2.23 Å and 2.25 Å. This can be understood as stemming from the coordination by ureas from different planes with unequal local coordination, as men-

tioned earlier. The Zn···Cl distance is shorter than in anhydrous crystalline $ZnCl_2$ (the δ phase, 2.265–2.282 Å) [59]. At the same time, it is appreciably longer than in the optimized gas phase $ZnCl_2$ (2.071 Å). Thus, the Zn···Cl bonds in the $ZnCl_2 \cdot 2\,CO(NH_2)_2$ proto-DES are closer to the ionic bonds in the crystal than to the covalent gas phase molecule.

Mulliken atomic charges in the studied crystal are compared with the respective charges in isolated component molecules in Table 3. The data for hydrogen atoms are omitted therein, but they show little variation in partial charge between different H atom types (0.367–0.370*e*). Concerning gas phase molecules, the most noticeable is the large degree of charge transfer from Cl to Zn in $ZnCl_2$, related to the strongly covalent character of the Zn–Cl bonds. In the crystal, the charge distribution around Zn(II) is much different, with zinc showing a more prominent ionic character and a 0.36*e* more positive charge than in isolated $ZnCl_2$. Apart from the more ionic character of Zn and Cl in the proto-DES, urea also shows an altered charge distribution with respect to the free molecule. Notably, the negative charge on O atoms is increased by ca. 0.04*e* due to coordination with Zn(II). However, the polarization of the C=O bond remains roughly the same, as measured by the partial charge difference on both atoms. A significant charge redistribution is observed on all four nonequivalent nitrogen atoms. The largest change in partial charge is noted for the N(1.2) atom, which is the center of the NH_2 group engaged in the urea dimer formation.

Table 3. Selected Mulliken atomic charges (in *e*) in the $ZnCl_2 \cdot 2\,CO(NH_2)_2$ crystal unit cell and its gas phase components.

Atom	$ZnCl_2 \cdot 2\,CO(NH_2)_2$	$ZnCl_2$	$CO(NH_2)_2$
Zn	1.337	0.974	
Cl(1)	−0.547	−0.487	
Cl(2)	−0.542	−0.487	
O(1)	−0.678		−0.633
O(2)	−0.672		−0.633
C(1)	0.616		0.706
C(2)	0.613		0.706
N(1.1)	−0.777		−0.941
N(1.2)	−0.756		−0.941
N(2.1)	−0.785		−0.941
N(2.2)	−0.761		−0.941

The lattice energy of the studied crystal was calculated per formula unit with respect to the isolated gas phase components from Equation (1):

$$\Delta_{lat}E = E_{supercell}/Z - E_{ZnCl_2} - 2E_{CO(NH_2)_2}\,, \quad (1)$$

where $E_{supercell}$, E_{ZnCl_2}, and $E_{CO(NH_2)_2}$ are the total energy of the supercell, zinc chloride molecule, and urea molecule, respectively, while Z is the number of formula units per supercell. The $\Delta_{lat}E$ value thus calculated is −3.996 eV (−385.5 kJ·mol^{-1}). For comparison, the lattice energy of urea is −0.969 eV (as obtained from its standard enthalpy of sublimation) [60]. As a consequence, each urea molecule in the studied crystal is stabilized by an additional 1.034 eV with respect to the pure urea crystal.

The formation of the $ZnCl_2 \cdot 2\,CO(NH_2)_2$ crystal is accompanied by a sizable deformation energy of the constituent molecules, which was calculated per formula unit from Equation (2):

$$\Delta_{def}E = E^{fix}_{ZnCl_2} - E_{ZnCl_2} + 2\left(E^{fix}_{CO(NH_2)_2} - E_{CO(NH_2)_2}\right), \quad (2)$$

where $E^{fix}_{ZnCl_2}$ and $E^{fix}_{CO(NH_2)_2}$ are the total energy of the zinc chloride molecule and urea molecule at the fixed geometry of the crystal. The calculated $\Delta_{def}E$ is 1.39 eV and as much as 73% of this value is attributable to the bending of $ZnCl_2$ (from the linear arrangement in the gas phase to 118.94° in the crystal).

To further characterize the energetic effects connected with the formation of the proto-DES crystal (treated as a cocrystal), we estimated its energy of formation from crystals of pure components by designing a suitable thermodynamic cycle; see Figure 4a. Accordingly, the desired value of $\Delta_{f,s}E(\mathrm{DES})$ was calculated from Equation (3):

$$\Delta_{f,s}E(\mathrm{DES}) = -\Delta_{lat}E(\mathrm{ZnCl_2(s)}) + 2\,\Delta_{sub}E(\mathrm{U\,(s)}) + \Delta_{lat}E(\mathrm{DES}) + \Delta_{f,i}E(\mathrm{ZnCl_2(g)})\,, \quad (3)$$

where $\Delta_{lat}E(\mathrm{ZnCl_2(s)})$ is the lattice energy of solid $ZnCl_2$ [61], $\Delta_{sub}E(\mathrm{U\,(s)})$ is the sublimation energy of urea [60], $\Delta_{lat}E(\mathrm{DES})$ is the lattice energy of the studied crystal obtained from Equation (1), and $\Delta_{f,i}E(\mathrm{ZnCl_2(g)})$ is the energy of formation of gaseous $ZnCl_2$ from the constituent ions, obtained from the cycle shown in Figure 4b, *vide infra*. The numerical values of all energies are given in Figure 4a and the obtained $\Delta_{f,s}E(\mathrm{DES})$ value is -0.744 eV, indicating the exothermic nature of the cocrystal formation process. We note here that the only parameter calculated in this work is the lattice energy of the $ZnCl_2(urea)_2$ obtained from Equation (1), while all others are standard thermodynamic data.

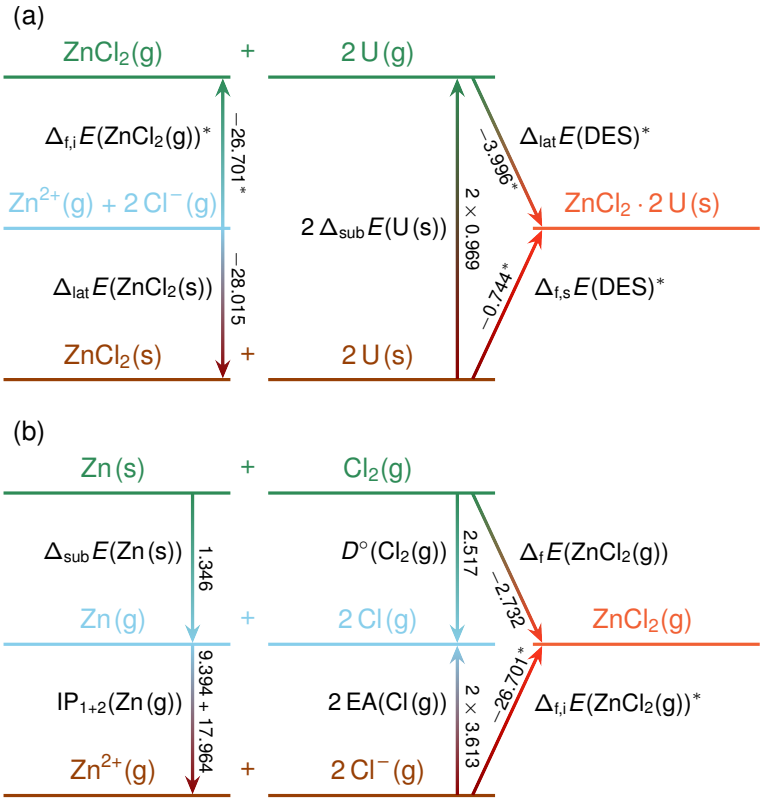


Figure 4. Thermodynamic cycles for estimation of (**a**) the formation energy of the $ZnCl_2 \cdot 2\,CO(NH_2)_2$ crystal from the crystalline molecular components, and (**b**) the formation energy of gaseous $ZnCl_2$ from the constituent ions. U—urea, *—values calculated in this work. All other energy values (in eV) were sourced from tabulated thermodynamic data [60–62]. See text for explanation of symbols.

The necessary value of $\Delta_{f,i}E(\mathrm{ZnCl_2(g)})$ was obtained from the cycle shown in Figure 4b and calculated from Equation (4):

$$\Delta_{f,i}E(\mathrm{ZnCl_2(g)}) = -\Delta_{sub}E(\mathrm{Zn\,(s)}) - \mathrm{IP_{1+2}(Zn\,(g))} - D^{\circ}(\mathrm{Cl_2(g)}) + 2\,\mathrm{EA(Cl\,(g))} + \Delta_{f}E(\mathrm{ZnCl_2(g)})\,, \quad (4)$$

where $\Delta_{sub}E(\mathrm{Zn\,(s)})$ is the sublimation energy of zinc chloride [62], $\mathrm{IP_{1+2}(Zn\,(g))}$ is the sum of the first two ionization energies of atomic zinc [61], $D^{\circ}(\mathrm{Cl_2(g)})$ is the bond dissociation energy of chlorine [61], $\mathrm{EA(Cl\,(g))}$ is the electron affinity of atomic chlorine [61], and $\Delta_{f}E(\mathrm{ZnCl_2(g)})$ is the standard energy of formation of gaseous $ZnCl_2$. The numerical values of these parameters are provided in Figure 4b.

The calculated IR spectrum of the crystal—without any scaling factor applied—is shown in Figure 5 and compared to the spectra of gas phase components. All spectra were broadened by 10 cm^{-1} full-width at half-maximum Gaussian bands, but individual transitions in the crystal are also indicated in the middle and right panels. We first focus on the right panel, which magnifies the NH_2 stretching vibration range. Gas phase urea shows two well-resolved vibrations, $\nu^{s}_{NH_2}$ at 3480 cm^{-1} and $\nu^{as}_{NH_2}$ at 3602 cm^{-1}. In the crystal, due to intermolecular interactions, primarily hydrogen bonding, these bands split into four transitions each and undergo a significant red shift. The most red-shifted band (at 3316 cm^{-1}) corresponds to the symmetric stretch of the NH_2 group that is engaged in the hydrogen-bonded urea dimer and also in the short HB to chloride (2.38 Å; see Figure 2a). The corresponding asymmetric stretch is found at 3444 cm^{-1}. The second NH_2 group of this urea molecule shows $\nu^{s}_{NH_2} = 3401$ cm^{-1} and $\nu^{as}_{NH_2} = 3523$ cm^{-1}. The remaining four transitions are symmetric and asymmetric NH_2 stretching vibrations of urea molecules located in the *b*-aligned plane.

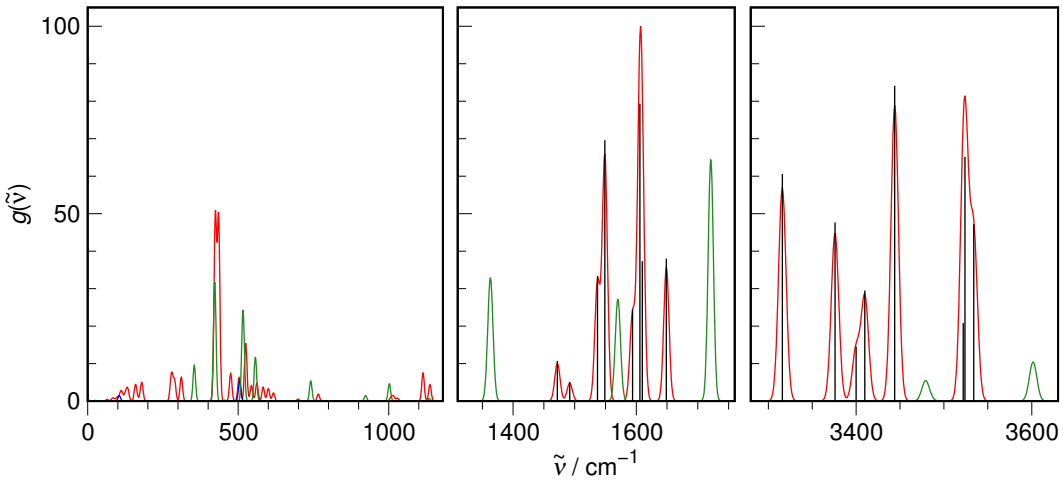


Figure 5. Calculated infrared spectra of the $ZnCl_2 \cdot 2\,CO(NH_2)_2$ crystal supercell (red), gas phase $ZnCl_2$ (blue), and gas phase urea (green) in the fingerprint region (**left**), the NH_2 bending and C=O stretching vibration range (**middle**), and the NH_2 stretching vibration range (**right**). The component spectra are multiplied by the number of respective molecules in the supercell. In the middle and right panels, black lines indicate individual transitions in the crystal.

The middle panel of Figure 5 focuses on the NH_2 bending and C=O stretching vibration range. In the gas phase, the most prominent band is the C=O stretch, located at 1722 cm^{-1}. In the crystal, it shifts significantly to red and splits into two transitions observed at 1538 and 1549 cm^{-1} for the two nonequivalent urea molecules. The most intensive band in the crystal (at 1607 cm^{-1}) is a combination of three closely laying NH_2 bending vibrations. The fourth one is slightly blue-shifted to 1650 cm^{-1} and can be ascribed to the strongest hydrogen-bonded NH_2 group engaged in the urea dimer. Thus, the four nonequivalent NH_2 groups in the crystal show uncoupled bending vibrations. The final band in this range is the ν^{as}_{NCN}, which is blue-shifted from 1364 cm^{-1} in the free molecule to 1473 and 1493 cm^{-1} and has a relatively small intensity. Again, the two nonequivalent urea molecules show well-resolved vibrational transitions.

In the fingerprint region, the most intense bands are wagging modes of the NH_2 groups, visible as a doublet at 424 and 436 cm^{-1}. Interestingly, the normal modes involving $ZnCl_2$, also expected there, show very small intensity and are barely visible, even after rescaling. The gas phase molecule shows the expected $\nu^{as}_{ZnCl_2}$ at 505 cm^{-1} and a doubly degenerate bending mode at 105 cm^{-1}. In the crystal, due to different local symmetries, both $\nu^{s}_{ZnCl_2}$ and $\nu^{as}_{ZnCl_2}$ are active and visible as two bands at 282 and 311 cm^{-1}, respectively, while the bending mode appears at 135 cm^{-1}.

It is instructive to compare the calculated IR spectrum with the case of crystalline urea [63]. There, the $\nu^{s}_{NH_2}$ and $\nu^{as}_{NH_2}$ bands are located at 3303 and 3336 cm^{-1} and 3451 and 3481 cm^{-1} (each band is split due to two different HB patterns in urea crystal, as discussed above). Therefore, only the strongest HB observed by us in the *c*-aligned dimer can match the situation in pure urea. Other HBs show a much smaller red shift from the gas phase position. On the contrary, the $\nu_{C=O}$ bands in $ZnCl_2 \cdot 2\,CO(NH_2)_2$ and crystalline urea have roughly the same position, the latter being located at 1540 cm^{-1} [63]. It is also worth comparing the $ZnCl_2$ band positions to experiment [64]. In crystalline α and β-$ZnCl_2$, as well as in the liquid, the stretching and bending modes are located at 260 cm^{-1} and 100 cm^{-1}, respectively, and the symmetric and asymmetric modes are not resolved. The band positions found by us are, again, much closer to the ionic crystal than to the covalent Zn–Cl bond in the gas phase.

4. Conclusions

In this work, we studied the $ZnCl_2(urea)_2$ crystal as a 'proto-DES' system using periodic density functional theory. The crystal possesses a molecular character, with Zn–Cl bonds showing partially ionic behavior. The two nonequivalent types of urea molecules are located on two perpendicular planes traceable in the crystal structure. One of them contains the repeating strongly hydrogen-bonded $(Cl^- \cdot CO(NH_2)_2)_2$ structural motif featuring a cyclic urea dimer. The interlocking planes are connected via tetrahedrally coordinated zinc cations. Non-covalent interaction analysis indicates that only the N–H···O hydrogen bonds in the dimer and the shortest of such bonds to chlorides can be classified as hydrogen bonds per se, the other displaying more of a van der Waals-type interactions character. Strong coordination interactions of two chlorides and two urea oxygen atoms with Zn(II) are revealed, however.

The calculated lattice energy of the studied crystal (vs. gas phase urea and $ZnCl_2$ as components) is ca. −4 eV per formula unit, but the energetic requirement of deforming the components to their geometry in the crystal is also large and endothermic and reaches almost 1.4 eV. The formation of $ZnCl_2(urea)_2$ treated as a cocrystal (i.e., from the crystalline components) is exothermic and equal −0.744 eV.

The calculated infrared spectrum of the $ZnCl_2(urea)_2$ crystal confirms differing chemical environment of each of the four nonequivalent NH_2 groups, revealing resolved sets of $\nu^{s}_{NH_2}$ and $\nu^{as}_{NH_2}$ bands for each. The hydrogen bonds, however, are generally weaker than in crystalline urea, with the exception of the ones holding the cyclic dimer, as evidenced by a smaller red shift from the gas phase free urea than in its crystal. The normal modes of $ZnCl_2$ in proto-DES are blue-shifted from its crystalline and liquid phases, confirming a slightly increased covalent character of the Zn–Cl bond.

Overall, the present investigation of the proto-DES crystal brings important implications for the structure of room-temperature liquids found at other compositions of this system:

- In $ZnCl_2$–urea systems, the N–H···Cl^- hydrogen bonds may compete with the possibly stronger N–H···O hydrogen bonds, leading to the formation of the 'urea subnetwork' in the structure of the liquid and poorer compatibility of the components. The appearance of cyclic urea dimers is a strong possibility.
- The N–H···Cl^- hydrogen bonds are expected to be bidentate, with a single urea molecule donating two such bonds to a chloride simultaneously. Such bonds are necessarily strained and far from linear and the urea–Cl^- interaction will be labile.
- The tetrahedral Zn(II) solvation complex with mixed coordination type, as seen in the crystal structure, is also possibly formed in the liquid DES, acting as a linker between the urea hydrogen bond network and the $ZnCl_2$ subsystem. The existence of other complex stoichiometries, such as $ZnCl^+(urea)_3$ and $ZnCl_3{}^-(urea)$ cannot be ruled out, however.
- The partially covalent character of the Zn–Cl bonds is probably responsible for the experimentally observed low conductivity of the $ZnCl_2$–urea DES, along with the

possibly dominating character of the electrically neutral coordination complexes, as found in the studied crystal.

- The comparison of the $ZnCl_2(urea)_2$ and pure urea crystal structures reveals that $ZnCl_2$ acts a a disruptor in the long-range hydrogen bond network formed by urea molecules, thus providing a natural explanation for the deep eutectic character of the system expressed via the significant lowering of the melting point.

To sum up, proto-DES crystalline systems provide a good model to study the dominant intermolecular interactions that probably carry on to the liquid phase DES. Whenever possible, they should be separately investigated in order to shine light on these interactions and provide guided guesstimates of the causes of DES fluidity. Computational investigations of such crystals using periodic DFT can further improve the understanding of interactions and be used, among others, to construct potential models that can be of use for the simulations of the respective liquid DESs.

Author Contributions: Conceptualization, M.Ś.; methodology, M.Ś.; supervision, M.Ś.; investigation, A.M.; formal analysis, A.M.; visualization, A.M.; writing—original draft preparation, A.M. and M.Ś.; writing—review and editing, A.M. and M.Ś. All authors have read and agreed to the published version of the manuscript.

Funding: This research received no external funding.

Data Availability Statement: The data presented in this study are available on request from the corresponding author.

Acknowledgments: Calculations were performed at the Academic Computer Center in Gdańsk (TASK).

Conflicts of Interest: The authors declare no conflicts of interest.

References

1. Smith, E.L.; Abbott, A.P.; Ryder, K.S. Deep Eutectic Solvents (DESs) and Their Applications. *Chem. Rev.* **2014**, *114*, 11060–11082. [CrossRef] [PubMed]
2. Abbott, A.P.; Capper, G.; Davies, D.L.; Rasheed, R.K.; Tambyrajah, V. Novel solvent properties of choline chloride/urea mixtures. *Chem. Commun.* **2003**, 70–71. [CrossRef] [PubMed]
3. Gilmore, M.; Swadzba-Kwasny, M.; Holbrey, J.D. Thermal Properties of Choline Chloride/Urea System Studied under Moisture-Free Atmosphere. *J. Chem. Eng. Data* **2019**, *64*, 5248–5255. [CrossRef]
4. van den Bruinhorst, A.; Avila, J.; Rosenthal, M.; Pellegrino, A.; Burghammer, M.; Costa Gomes, M. Defying decomposition: The curious case of choline chloride. *Nat. Commun.* **2023**, *14*, 6684. [CrossRef] [PubMed]
5. Chen, Y.; Yu, D.; Chen, W.; Fu, L.; Mu, T. Water absorption by deep eutectic solvents. *Phys. Chem. Chem. Phys.* **2019**, *21*, 2601–2610. [CrossRef] [PubMed]
6. Palmelund, H.; Rantanen, J.; Löbmann, K. Deliquescence Behavior of Deep Eutectic Solvents. *Appl. Sci.* **2021**, *11*, 1601. [CrossRef]
7. Hansen, B.B.; Spittle, S.; Chen, B.; Poe, D.; Zhang, Y.; Klein, J.M.; Horton, A.; Adhikari, L.; Zelovich, T.; Doherty, B.W.; et al. Deep Eutectic Solvents: A Review of Fundamentals and Applications. *Chem. Rev.* **2021**, *121*, 1232–1285. [CrossRef]
8. Abranches, D.O.; Martins, M.A.R.; Silva, L.P.; Schaeffer, N.; Pinho, S.P.; Coutinho, J.A.P. Phenolic hydrogen bond donors in the formation of non-ionic deep eutectic solvents: The quest for type V DES. *Chem. Commun.* **2019**, *55*, 10253–10256. [CrossRef]
9. Ünlü, A.E.; Arıkaya, A.; Takaç, S. Use of deep eutectic solvents as catalyst: A mini-review. *Green Process. Synth.* **2019**, *8*, 355–372. [CrossRef]
10. Yu, D.; Xue, Z.; Mu, T. Deep eutectic solvents as a green toolbox for synthesis. *Cell Rep. Phys. Sci.* **2022**, *3*, 100809. [CrossRef]
11. Rodríguez-Llorente, D.; Cañada-Barcala, A.; Álvarez Torrellas, S.; Águeda, V.I.; García, J.; Larriba, M. A Review of the Use of Eutectic Solvents, Terpenes and Terpenoids in Liquid–liquid Extraction Processes. *Processes* **2020**, *8*, 1220. [CrossRef]
12. Shishov, A.; Bulatov, A.; Locatelli, M.; Carradori, S.; Andruch, V. Application of deep eutectic solvents in analytical chemistry. A review. *Microchem. J.* **2017**, *135*, 33–38. [CrossRef]
13. Płotka-Wasylka, J.; De La Guardia, M.; Andruch, V.; Vilková, M. Deep eutectic solvents vs. ionic liquids: Similarities and differences. *Microchem. J.* **2020**, *159*, 105539. [CrossRef]
14. Abo-Hamad, A.; Hayyan, M.; AlSaadi, M.A.; Hashim, M.A. Potential applications of deep eutectic solvents in nanotechnology. *Chem. Eng. J.* **2015**, *273*, 551–567. [CrossRef]
15. Chakrabarti, M.H.; Mjalli, F.S.; AlNashef, I.M.; Hashim, M.A.; Hussain, M.A.; Bahadori, L.; Low, C.T.J. Prospects of applying ionic liquids and deep eutectic solvents for renewable energy storage by means of redox flow batteries. *Renew. Sustain. Energy Rev.* **2014**, *30*, 254–270. [CrossRef]

16. Zhang, Q.; De Oliveira Vigier, K.; Royer, S.; Jérôme, F. Deep eutectic solvents: Syntheses, properties and applications. *Chem. Soc. Rev.* **2012**, *41*, 7108. [CrossRef] [PubMed]
17. Morozova, O.V.; Vasil'eva, I.S.; Shumakovich, G.P.; Zaitseva, E.A.; Yaropolov, A.I. Deep Eutectic Solvents for Biotechnology Applications. *Biochemistry* **2023**, *88*, S150–S175. [CrossRef] [PubMed]
18. Khalid, A.; Tahir, S.; Khalid, A.R.; Hanif, M.A.; Abbas, Q.; Zahid, M. Breaking new grounds: Metal salts based-deep eutectic solvents and their applications- a comprehensive review. *Green Chem.* **2024**, *26*, 2421–2453. [CrossRef]
19. Abbott, A.P.; Barron, J.C.; Ryder, K.S.; Wilson, D. Eutectic-Based Ionic Liquids with Metal-Containing Anions and Cations. *Chem. Eur. J.* **2007**, *13*, 6495–6501. [CrossRef]
20. Lian, H.; Hong, S.; Carranza, A.; Mota-Morales, J.D.; Pojman, J.A. Processing of lignin in urea–zinc chloride deep-eutectic solvent and its use as a filler in a phenol-formaldehyde resin. *RSC Adv.* **2015**, *5*, 28778–28785. [CrossRef]
21. Gao, J.; Lin, H.; Wen, A.; Chen, J.; Yang, W.; Li, R. Zinc Complex Derived from ZnCl2-Urea Ionic Liquid for Improving Mildew Property of Bamboo. *Coatings* **2020**, *10*, 1233. [CrossRef]
22. Li, X.; Xiao, J.; Wei, W.; Yan, M.; Guo, D.; Lian, H. Preparation mechanism and performance evaluation of deep eutectic solvent-lignin/ZnO composites by one-pot. *Int. J. Biol. Macromol.* **2023**, *225*, 1405–1414. [CrossRef]
23. Ochoa-Puentes, C.; Higuera, N.; Peña-Solórzano, D. Urea–Zinc Chloride Eutectic Mixture-Mediated One-Pot Synthesis of Imidazoles: Efficient and Ecofriendly Access to Trifenagrel. *Synlett* **2018**, *30*, 225–229. [CrossRef]
24. Nishtala, V.B.; Basavoju, S. ZnCl2+Urea, the deep eutectic solvent promoted synthesis of the spirooxindolopyrans and xanthenes through a pseudo-three-component approach. *Synth. Commun.* **2019**, *49*, 2342–2349. [CrossRef]
25. Aghapoor, K.; Mohsenzadeh, F.; Darabi, H.R.; Sayahi, H.; Jalali, M.R. ZnCl2/Urea Eutectic Solvent as Stable Carbonylation Source for Benign Synthesis of 2–Benzimidazolones and 2–Imidazolones: An Effective Strategy for Preventing NH3 Gas Evolution. *ChemistrySelect* **2019**, *4*, 11093–11097. [CrossRef]
26. Peña-Solórzano, D.; Kouznetsov, V.V.; Ochoa-Puentes, C. Physicochemical properties of a urea/zinc chloride eutectic mixture and its improved effect on the fast and high yield synthesis of indeno[2,1-*C*]quinolines. *New J. Chem.* **2020**, *44*, 7987–7997. [CrossRef]
27. Walvekar, R.; Kunju, K.; Saputra, R.; Siddiqui, K.; Ramarad, S. Parametric Study for Devulcanization of Waste Tire Rubber Utilizing Deep Eutectic Solvent (DES). *MATEC Web Conf.* **2018**, *152*, 01005. [CrossRef]
28. Wang, Q.; Yao, X.; Geng, Y.; Zhou, Q.; Lu, X.; Zhang, S. Deep eutectic solvents as highly active catalysts for the fast and mild glycolysis of poly(ethylene terephthalate)(PET). *Green Chem.* **2015**, *17*, 2473–2479. [CrossRef]
29. Gontrani, L.; Donia, D.T.; Maria Bauer, E.; Tagliatesta, P.; Carbone, M. Novel Synthesis of Zinc Oxide Nanoparticles from Type IV Deep Eutectic Solvents. *Inorg. Chim. Acta* **2023**, *545*, 121268. [CrossRef]
30. Rong, K.; Huang, L.; Zhang, H.; Zhai, J.; Fang, Y.; Dong, S. Electrochemical fabrication of nanoporous gold electrodes in a deep eutectic solvent for electrochemical detections. *Chem. Commun.* **2018**, *54*, 8853–8856. [CrossRef]
31. Wang, L.; Deng, Y.; Yan, L. Low-Cost "Water-in-Deep Eutectic Solvent" Electrolyte for High-Performance Zinc Ion Hybrid Supercapacitors. *ACS Appl. Energy Mater.* **2023**, *6*, 10585–10592. [CrossRef]
32. Tolmachev, D.; Lukasheva, N.; Ramazanov, R.; Nazarychev, V.; Borzdun, N.; Volgin, I.; Andreeva, M.; Glova, A.; Melnikova, S.; Dobrovskiy, A.; et al. Computer Simulations of Deep Eutectic Solvents: Challenges, Solutions, and Perspectives. *Int. J. Mol. Sci.* **2022**, *23*, 645. [CrossRef] [PubMed]
33. Velez, C.; Acevedo, O. Simulation of deep eutectic solvents: Progress to promises. *Wiley Interdiscip. Rev. Comput. Mol. Sci.* **2022**, *12*, e1598. [CrossRef]
34. Zahn, S.; Kirchner, B.; Mollenhauer, D. Charge Spreading in Deep Eutectic Solvents. *ChemPhysChem* **2016**, *17*, 3354–3358. [CrossRef]
35. Alizadeh, V.; Malberg, F.; Pádua, A.A.H.; Kirchner, B. Are There Magic Compositions in Deep Eutectic Solvents? Effects of Composition and Water Content in Choline Chloride/Ethylene Glycol from Ab Initio Molecular Dynamics. *J. Phys. Chem. B* **2020**, *124*, 7433–7443. [CrossRef]
36. Abranches, D.O.; Coutinho, J.A. Everything You Wanted to Know about Deep Eutectic Solvents but Were Afraid to Be Told. *Annu. Rev. Chem. Biomol. Eng.* **2023**, *14*, 141–163. [CrossRef] [PubMed]
37. Agieienko, V.; Buchner, R. Is ethaline a deep eutectic solvent? *Phys. Chem. Chem. Phys.* **2022**, *24*, 5265–5268. [CrossRef] [PubMed]
38. Mishra, D.K.; Gopakumar, G.; Pugazhenthi, G.; Siva Brahmmananda Rao, C.V.; Nagarajan, S.; Banerjee, T. Molecular and Spectroscopic Insights into a Metal Salt-Based Deep Eutectic Solvent: A Combined Quantum Theory of Atoms in Molecules, Noncovalent Interaction, and Density Functional Theory Study. *J. Phys. Chem. A* **2021**, *125*, 9680–9690. [CrossRef]
39. Singh, M.B.; Kumar, A.; Jain, P.; Singh, P.; Kumari, K. An insight of novel eutectic mixture between thiazolidine-2,4-dione and zinc chloride: Temperature-dependent density functional theory approach. *J. Phys. Org. Chem.* **2021**, *35*, e4305. [CrossRef]
40. Furmanova, N.G.; Resnyanski, V.F.; Sulaimankulov, K.S.; Sulaimankulova, D.K.; Zhorobekova, S.Z. Crystal structure of the zinc chloride complex with carbamide, $ZnCl_2 \cdot 2\,CO(NH_2)_2$. *Crystallogr. Rep.* **1998**, *43*, 234–236.
41. Furmanova, N.G.; Resnyanski, V.F.; Sulaimankulov, K.S.; Zhorobekova, S.Z.; Sulaimankulova, D.K. Crystal structure of the zinc iodide complex with carbamide, $ZnI_2 \cdot 2\,CO(NH_2)_2$. *Crystallogr. Rep.* **2001**, *46*, 51–55. [CrossRef]
42. Erkasov, R.S.; Nesmeyanova, R.M.; Orazbaeva, R.S.; Bolysbekova, S.M. Solubility in the $ZnCl_2 - CO(NH_2)_2 - HCl - H_2O$ system at 25 °C. *Russ. J. Inorg. Chem.* **2013**, *58*, 213–215. [CrossRef]
43. Groom, C.R.; Bruno, I.J.; Lightfoot, M.P.; Ward, S.C. The Cambridge Structural Database. *Acta Crystallogr. B* **2016**, *72*, 171–179. [CrossRef] [PubMed]

44. Clark, S.J.; Segall, M.D.; Pickard, C.J.; Hasnip, P.J.; Probert, M.J.; Refson, K.; Payne, M. First principles methods using CASTEP. *Z. Kristall.* **2005**, *220*, 567–570. [CrossRef]
45. Perdew, J.P.; Burke, K.; Ernzerhof, M. Generalized Gradient Approximation Made Simple. *Phys. Rev. Lett.* **1996**, *77*, 3865–3868. [CrossRef] [PubMed]
46. Grimme, S.; Antony, J.; Ehrlich, S.; Krieg, H. A consistent and accurate ab initio parametrization of density functional dispersion correction (DFT-D) for the 94 elements H-Pu. *J. Chem. Phys.* **2010**, *132*, 154104. [CrossRef] [PubMed]
47. Grimme, S.; Ehrlich, S.; Goerigk, L. Effect of the damping function in dispersion corrected density functional theory. *J. Comput. Chem.* **2011**, *32*, 1456–1465. [CrossRef] [PubMed]
48. Hamann, D.R.; Schluter, M.; Chiang, C. Norm-Conserving Pseudopotentials. *Phys. Rev. Lett.* **1979**, *43*, 1494–1497. [CrossRef]
49. Monkhorst, H.J.; Pack, J.D. Special points for Brillouin-zone integrations. *Phys. Rev. B* **1976**, *13*, 5188–5192. [CrossRef]
50. Björkman, T. CIF2Cell: Generating geometries for electronic structure programs. *Comput. Phys. Commun.* **2011**, *182*, 1183–1186. [CrossRef]
51. Bader, R.F.W. A quantum theory of molecular structure and its applications. *Chem. Rev.* **1991**, *91*, 893–928. [CrossRef]
52. Johnson, E.R.; Keinan, S.; Mori-Sánchez, P.; Contreras-García, J.; Cohen, A.J.; Yang, W. Revealing Noncovalent Interactions. *J. Am. Chem. Soc.* **2010**, *132*, 6498–6506. [CrossRef] [PubMed]
53. Otero-de-la-Roza, A.; Johnson, E.R.; Luaña, V. CRITIC2: A program for real-space analysis of quantum chemical interactions in solids. *Comput. Phys. Commun.* **2014**, *185*, 1007–1018. [CrossRef]
54. Otero-de-la-Roza, A.; Blanco, M.A.; Pendás, A.M.; Luaña, V. Critic: A new program for the topological analysis of solid-state electron densities. *Comput. Phys. Commun.* **2009**, *180*, 157–166. [CrossRef]
55. Rutter, M.J. C2x: A tool for visualisation and input preparation for CASTEP and other electronic structure codes. *Comput. Phys. Commun.* **2018**, *225*, 174–179. [CrossRef]
56. Humphrey, W.; Dalke, A.; Schulten, K. VMD—Visual Molecular Dynamics. *J. Mol. Graph.* **1996**, *14*, 33–38. [CrossRef] [PubMed]
57. Emamian, S.; Lu, T.; Kruse, H.; Emamian, H. Exploring Nature and Predicting Strength of Hydrogen Bonds: A Correlation Analysis Between Atoms-in-Molecules Descriptors, Binding Energies, and Energy Components of Symmetry-Adapted Perturbation Theory. *J. Comput. Chem.* **2019**, *40*, 2868–2881. [CrossRef] [PubMed]
58. Zavodnik, V.; Stash, A.; Tsirelson, V.; de Vries, R.; Feil, D. Electron density study of urea using TDS-corrected X-ray diffraction data: Quantitative comparison of experimental and theoretical results. *Acta Crystallogr. B* **1999**, *55*, 45–54. [CrossRef]
59. Yakel, H.L.; Brynestad, J. Refinement of the crystal structure of orthorhombic zinc chloride. *Inorg. Chem.* **1978**, *17*, 3294–3296. [CrossRef]
60. Emel'yanenko, V.N.; Kabo, G.J.; Verevkin, S.P. Measurement and Prediction of Thermochemical Properties: Improved Increments for the Estimation of Enthalpies of Sublimation and Standard Enthalpies of Formation of Alkyl Derivatives of Urea. *J. Chem. Eng. Data* **2006**, *51*, 79–87. [CrossRef]
61. Haynes, W.M. (Ed.) *CRC Handbook of Chemistry and Physics*, 95th ed.; CRC Press: Boca Raton, FL, USA, 2014.
62. McCreary, J.R.; Thorn, R.J. Enthalpy of Sublimation of Zinc and Cadmium; Correlation of ΔH° vs. ΔS°; Comparison of Torsional and Knudsen Vapor Pressures. *J. Chem. Phys.* **1969**, *50*, 3725–3733.
63. Timón, V.; Maté, B.; Herrero, V.J.; Tanarro, I. Infrared spectra of amorphous and crystalline urea ices. *Phys. Chem. Chem. Phys.* **2021**, *23*, 22344–22351. [CrossRef] [PubMed]
64. Angell, C.; Wegdam, G.; van der Elsken, J. FIR spectra of liquid, glass and crystalline states of $ZnCl_2$: Order and temperature effects on band shape. *Spectrochim. Acta A* **1974**, *30*, 665–672. [CrossRef]

Disclaimer/Publisher's Note: The statements, opinions and data contained in all publications are solely those of the individual author(s) and contributor(s) and not of MDPI and/or the editor(s). MDPI and/or the editor(s) disclaim responsibility for any injury to people or property resulting from any ideas, methods, instructions or products referred to in the content.